ChemCatChem

Supporting Information

Effect of Metal Layer Support Structures on the Catalytic Activity of NiFe(oxy)hydroxide (LDH) for the OER in Alkaline Media

Christopher Gort[+],* Paul W. Buchheister[+], Malte Klingenhof, Stephen D. Paul, Fabio Dionigi, Roel van de Krol, Ulrike I. Kramm, Wolfram Jaegermann, Jan P. Hofmann,* Peter Strasser,* and Bernhard Kaiser

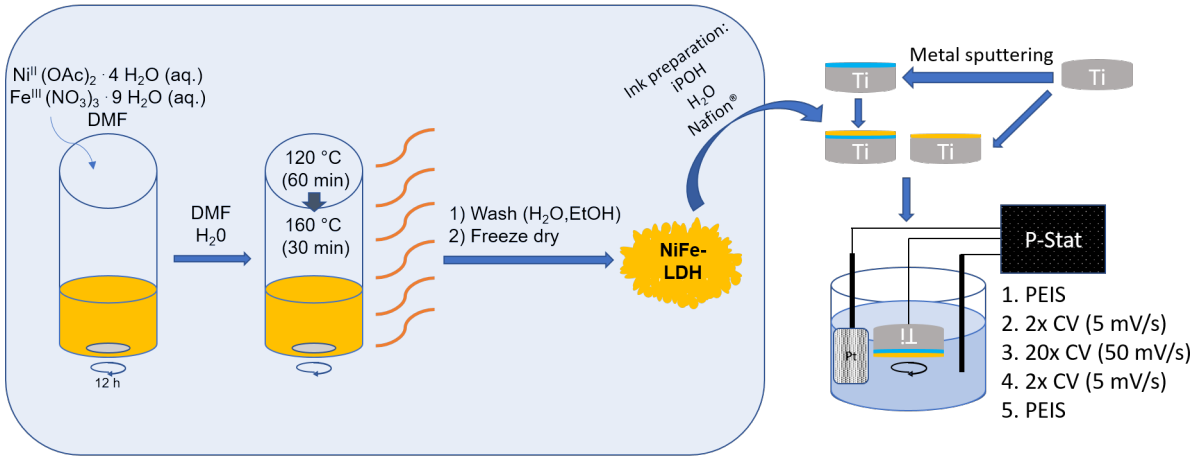

Fig. S 1: Synthesis route and electrochemical analysis for NiFe LDH. Nickel acetate and iron nitrate are hydrolyzed and stirred in a solution of DMF for 12h. Next the catalyst solution is heated with a microwave up to 120°C for 60 min, follow by 160°C for 30 min. After washing and freeze drying the catalyst solution an ink solution is obtained which can be deposited onto the metal coated or uncoated substrates.

Electrochemical activation procedures

Compared to the NiFe LDH samples, the activation routine for the thin film samples consisted of 5 cycles at a scan rate of 5 mV/s, 50 cycles at 50 mV/s and again 5 cycles at 5 mV/s. For each cycle, the voltage interval was 1.1-1.8 V vs. RHE, where 1.8 V vs. RHE was also the end point of each CV.

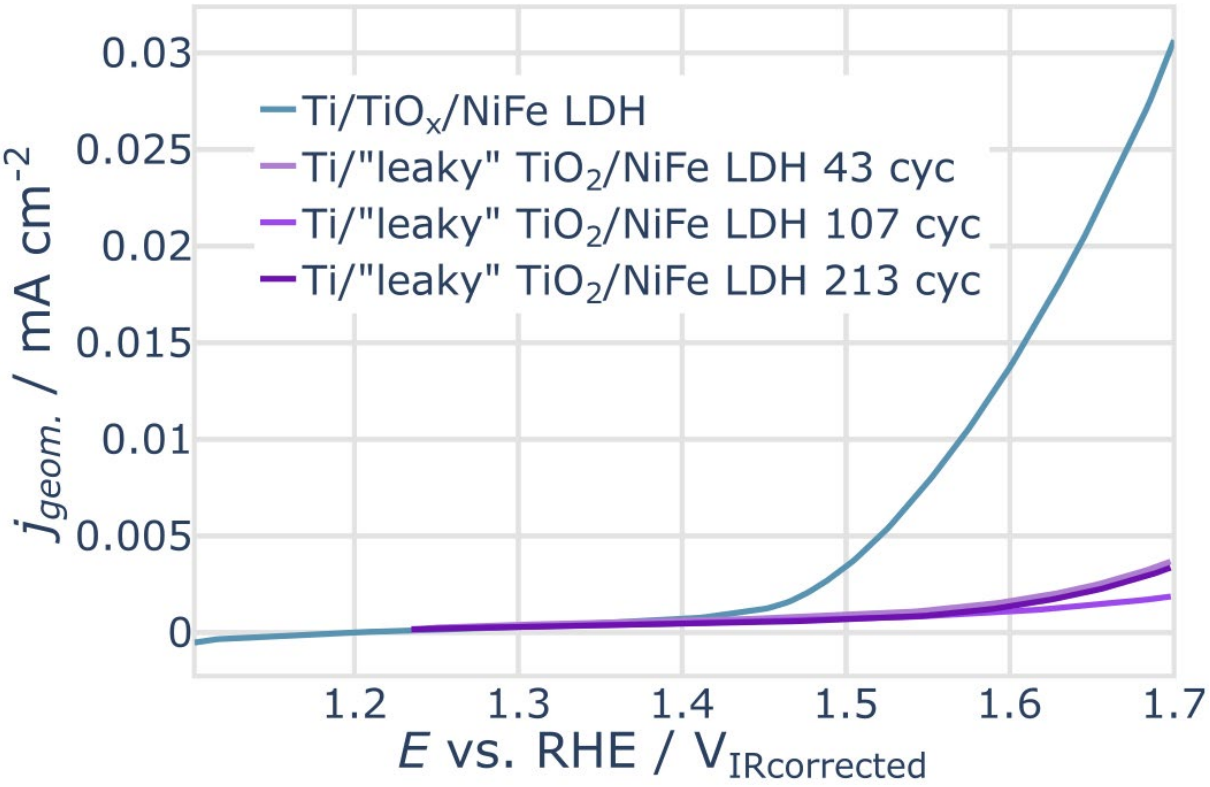

Fig. S 2: OER activity at RT of NiFe LDH on different titania supports. For comparison the CV after several cycles are shown for a “leaky” titania substrate.

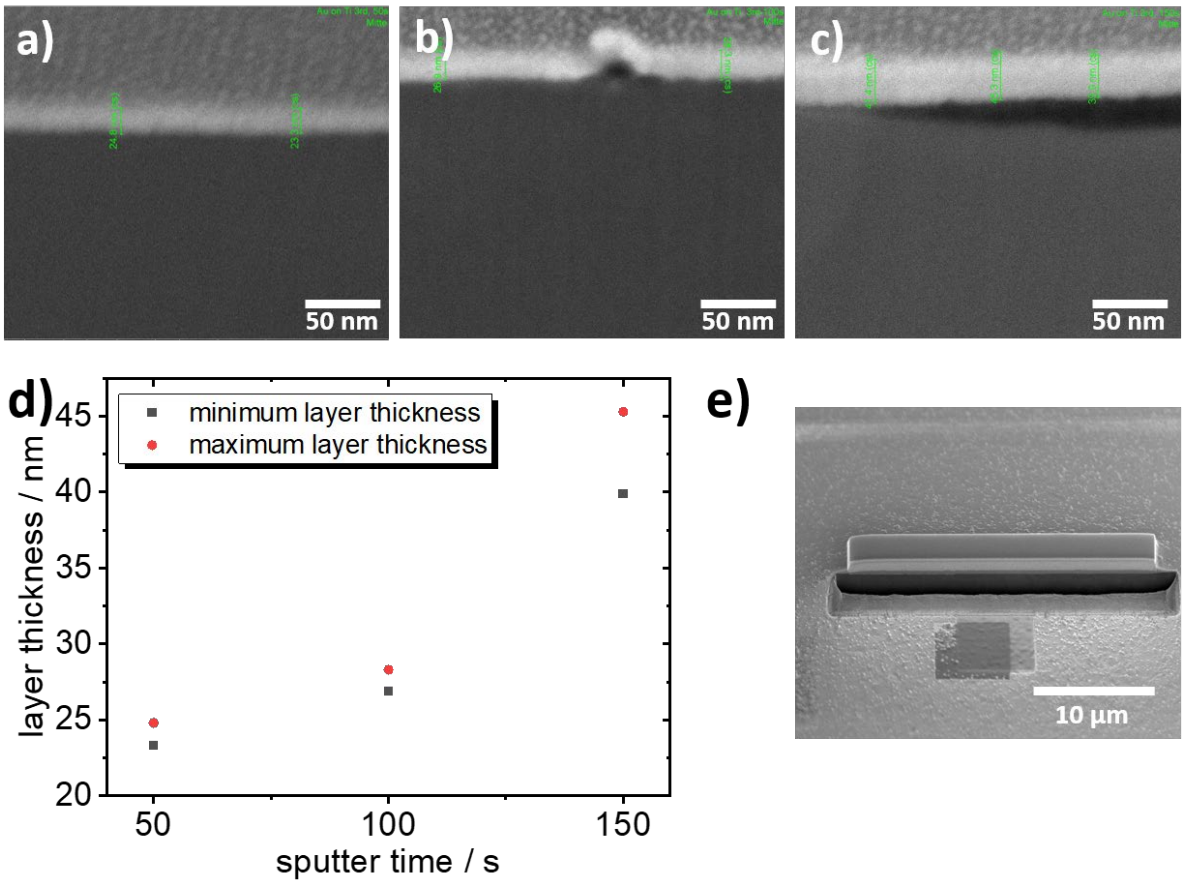

Fig. S 3 I: SEM images of sputter-deposited Au layers on Ti: a) Ti/TiO_x/Au (50 s) b) SEM of Ti/TiO_x/Au (100 s) c) SEM of Ti/TiO_x/Au (150 s). Possible starting points of layer delamination are visible d) Sputter times and corresponding layer thickness in the middle of the electrode, e) SEM of the FIB lamella used to determine the layer thickness.

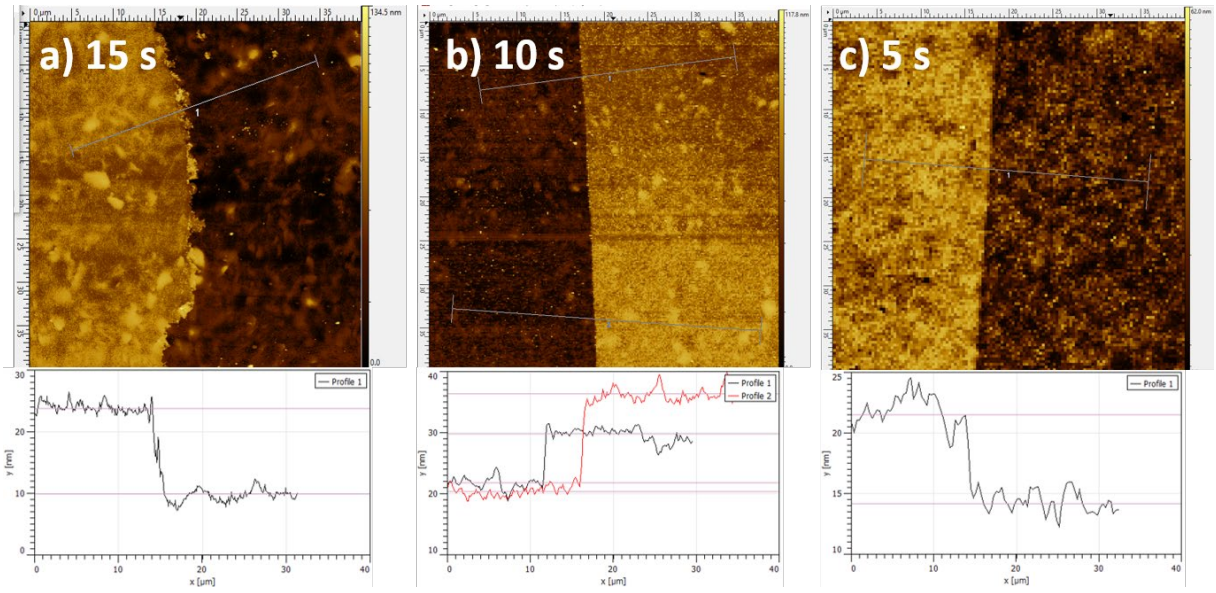

Fig. S 3 II: AFM-Measurement of sputter-deposited Au layers on Ti: a) Ti/TiO_x/Au (15 s) b) Ti/TiO_x/Au (10 s) c) Ti/TiO_x/Au (5s)

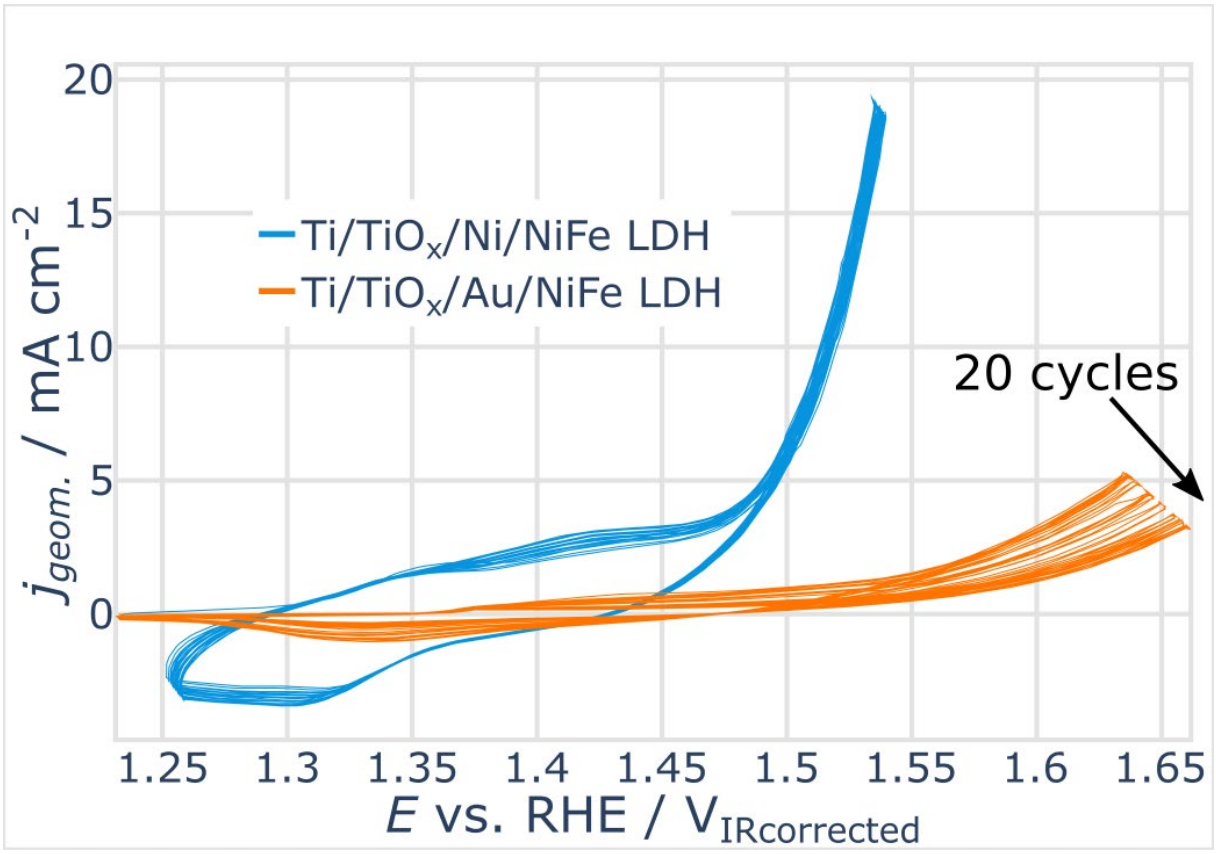

Fig. S 4: Stability at RT of NiFe LDH on metal sputtered titania electrodes during the activation cycles. 0.1 M KOH was used as electrolyte.

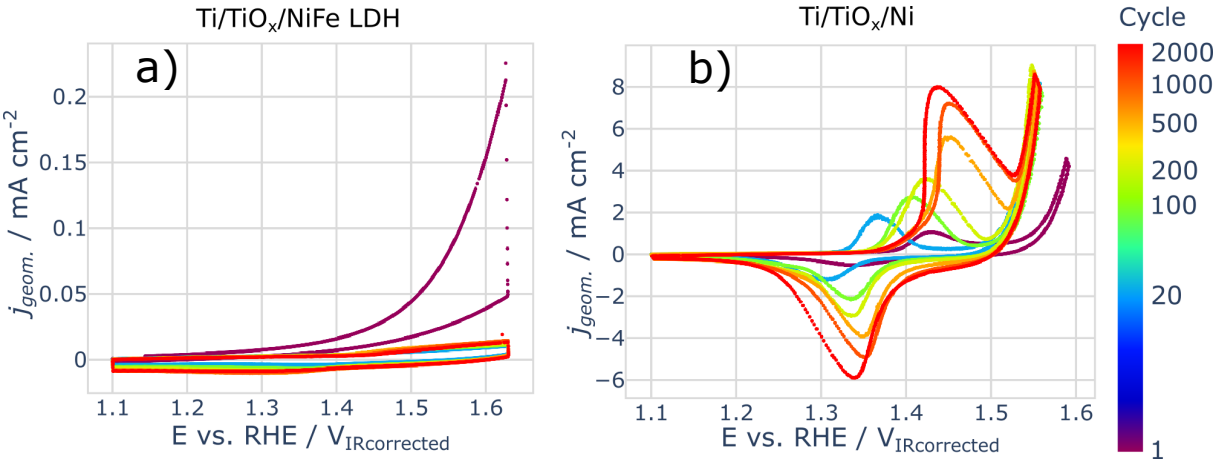

Fig. S 5: Accelerated stress test of the as prepared electrodes consisting of 2000 CVs in an RDE setup with a holding time of 10 s at the beginning and end of each scan. a) Ti/TiOx/NiFe LDH, b) Ti/TiOx/Ni

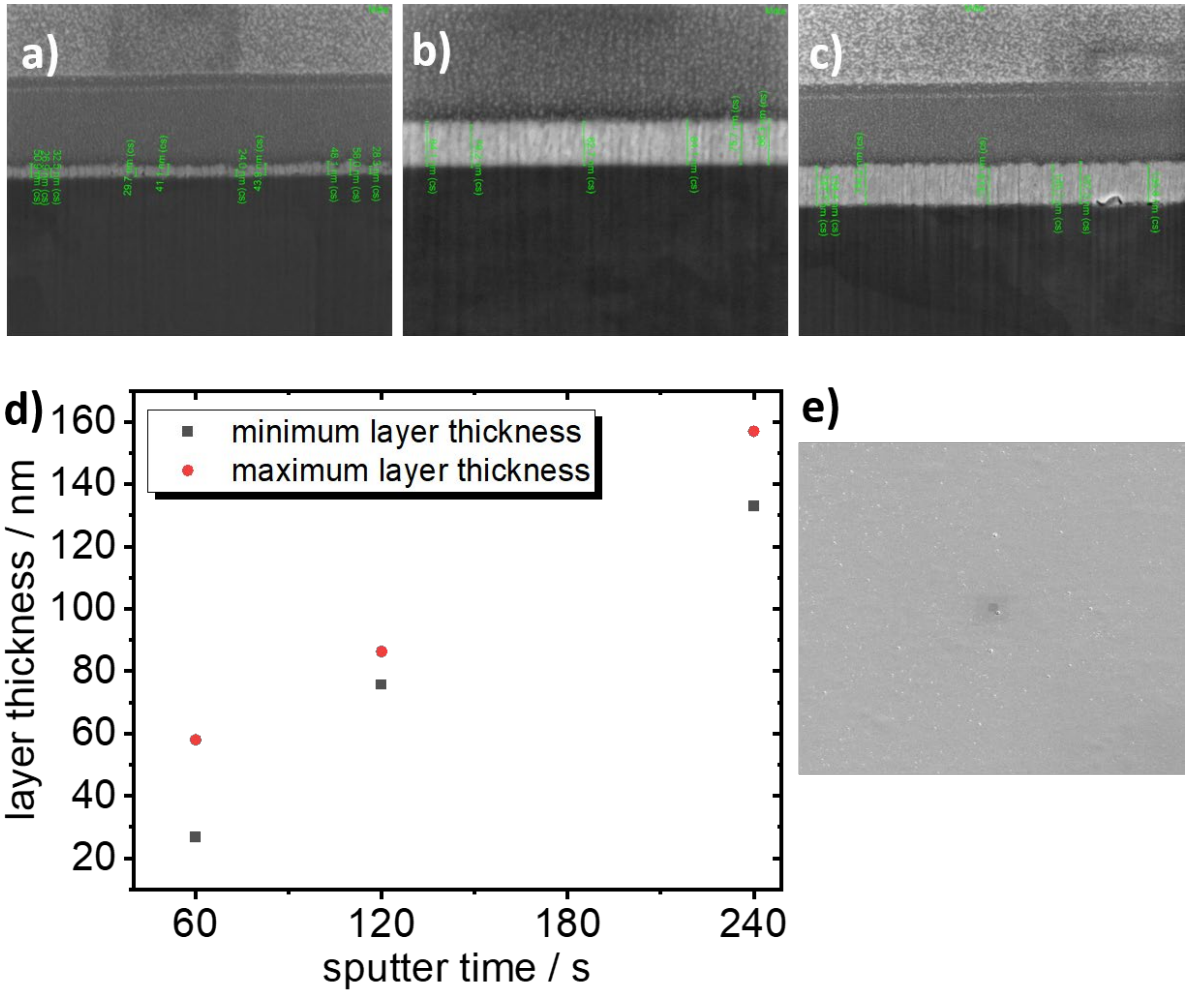

Fig. S 6 I: a) SEM of Ti/TiO_x/Ni (60 s) b) SEM of Ti/TiO_x/Au (120 s) c) SEM of Ti/TiO_x/Au (240 s). d) Sputter times and corresponding layer thickness in the middle of the electrode, e) SEM of the surface of the electrode showing roughing of the electrode surface increasing the available area.

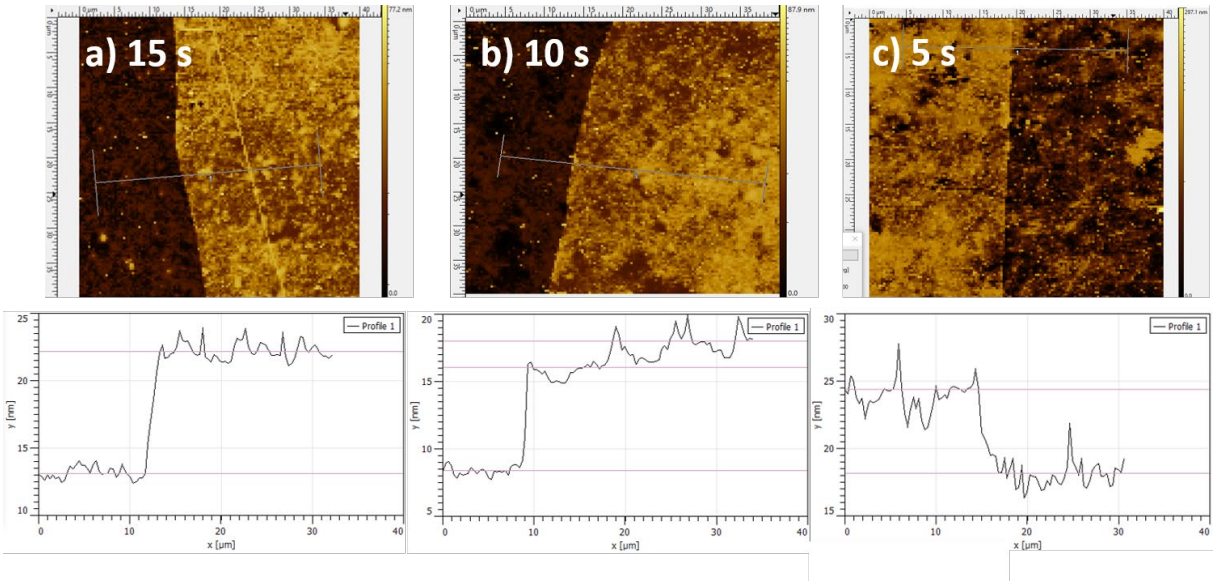

Fig. S 6 II: AFM-Measurement of sputter-deposited Ni layers on Ti: a) Ti/TiO_x/Ni (15 s) b) Ti/TiO_x/Ni (10 s) c) Ti/TiO_x/Ni (5s)

Table S 1: Interlayer thicknesses deposited at various sputter times measured with AFM

		Interlayer Metal	
		Au	**Ni**
Sputter Time	**5 s**	7 ± 1	4.5 ± 1.5
	10 s	12 ± 3	8 ± 1
	15 s	13 ± 1	9.5 ± 0.5
	50 s	24 ± 1	45 ± 15
	100 s	27 ± 2	80 ± 5
	150 s	42 ± 3	145 ± 12
		Interlayer Thickness / nm	

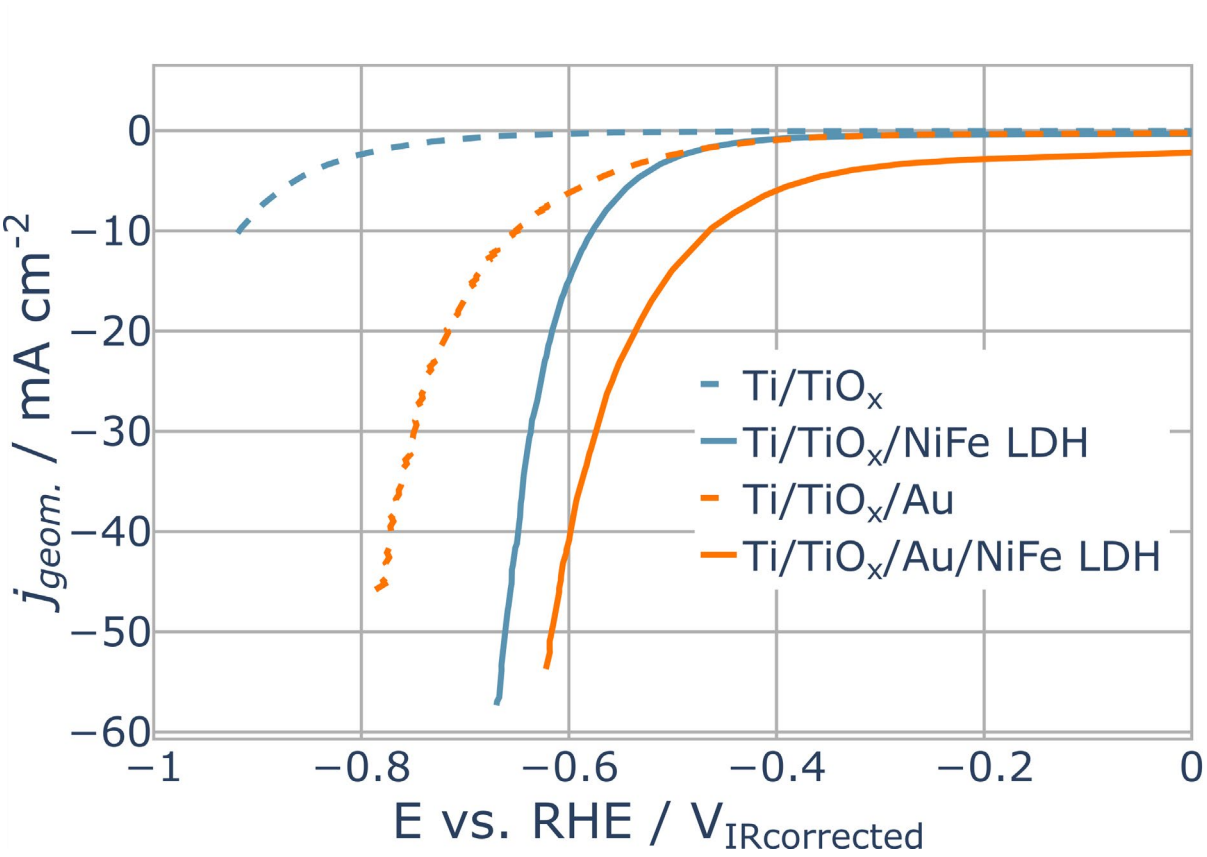

Fig. S 7: HER activity of various titania electrodes. Experiments were performed at RT in 0.1 M KOH as electrolyte.

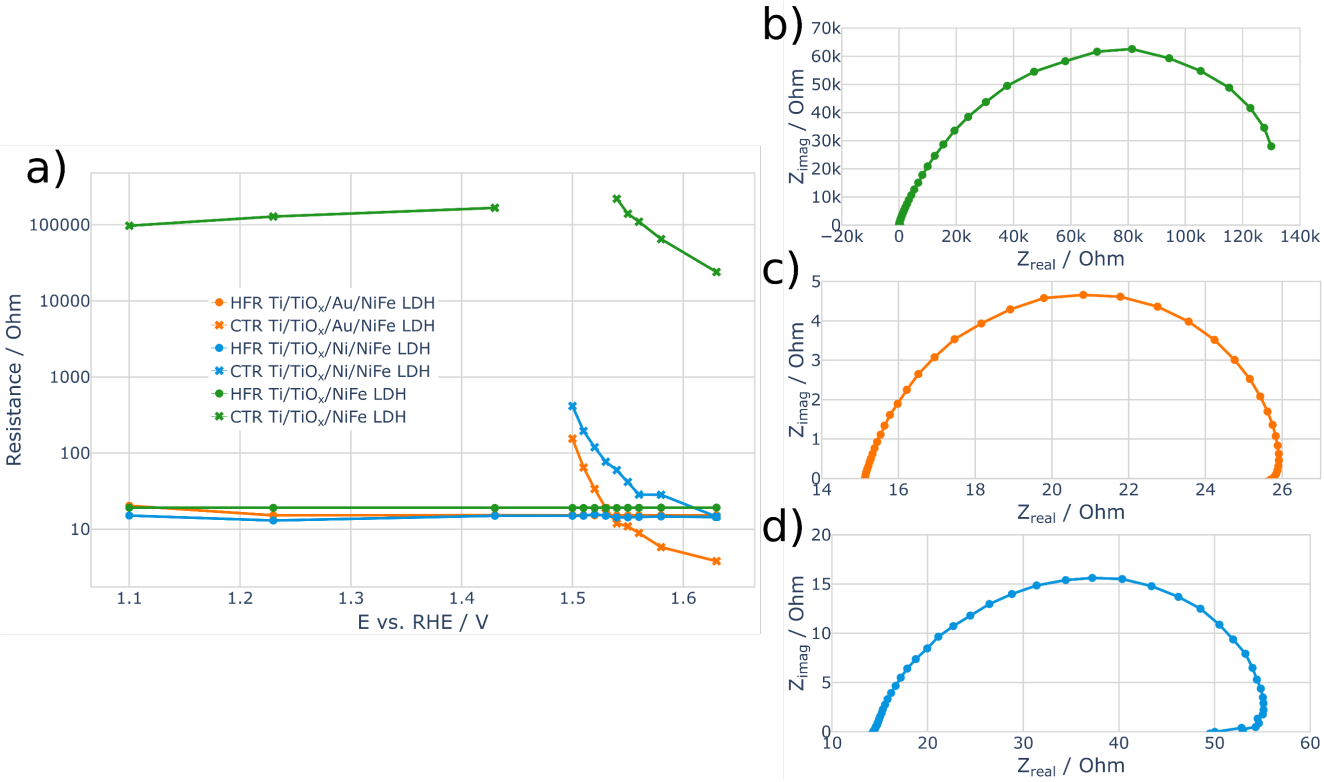

Fig. S 8: Electrochemical impedance spectroscopy measured on different electrodes. a) Potential dependent high frequency resistance (HFR) and charge transfer resistance (CTR) of the investigated electrodes. Values for the HFR and CTR were extracted from the Nyquist Plots utilizing the first (HFR) and last (CTR) intersection of the Nyquist Plot with the X-axis. b-d) exemplary Nyquist Plots for the three electrodes at 1.53 V vs. RHE in 0.1 M KOH. b) Ti/TiO_x/NiFe LDH, c) Ti/TiO_x/Au/NiFe LDH, d) Ti/TiO_x/Ni/NiFe LDH

While the HFR of all the investigated electrodes is similar and mostly dependent on the distance between electrode and Luggin capillary, the difference in the CTR is two orders of magnitudes. This implies that the resistivity of the support, which is (next to the resistance of the electrolyte and the cabling) included in the HFR and eliminated by IR-Correction, is not the main reason for the poor activity of NiFe LDH on titanium substrates, but rather that charge transfer is hindered for Ti/TiO_x/NiFe LDH.

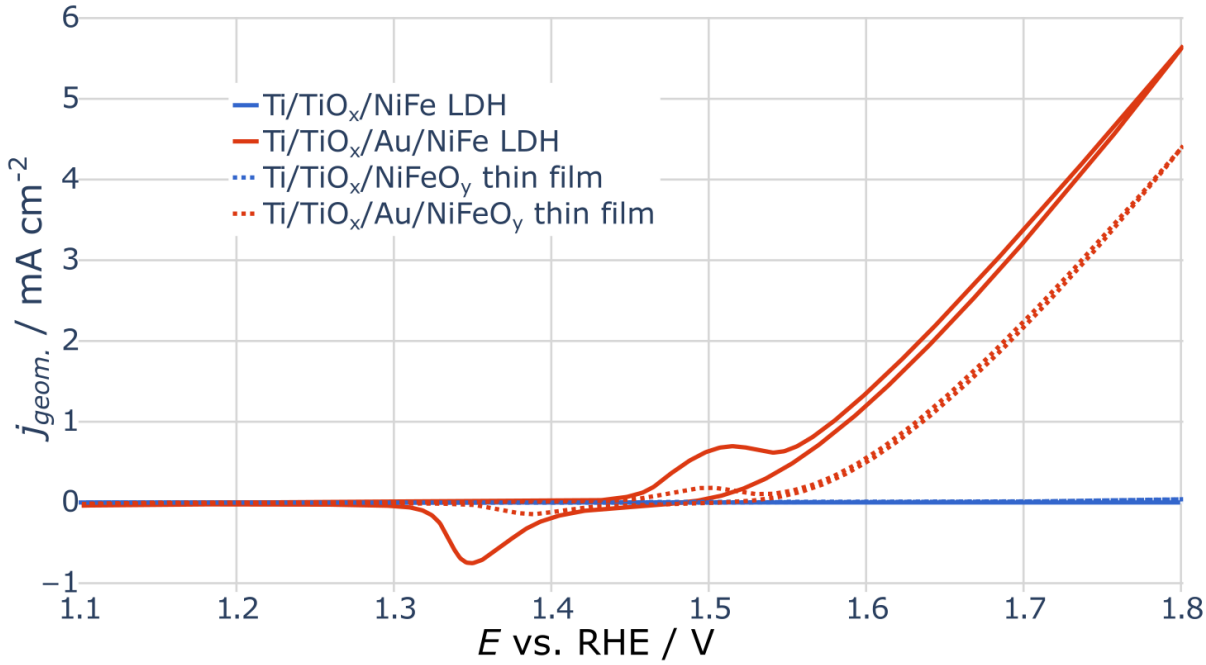

Fig. S 9: Comparison of the CV curves for the different materials synthesized by the various methods used, measured under identical conditions with the same setup. The curves for the solvothermal prepared Ti/TiOx/NiFe LDH (blue) and the thin film Ti/TiOx/NiFeOx (orange) samples without the gold layer are only visible as baselines at the selected vertical scale. The preparation method has only a small influence on the OER activity, the dominant factor for device performance remains the inclusion of the gold interlayer.

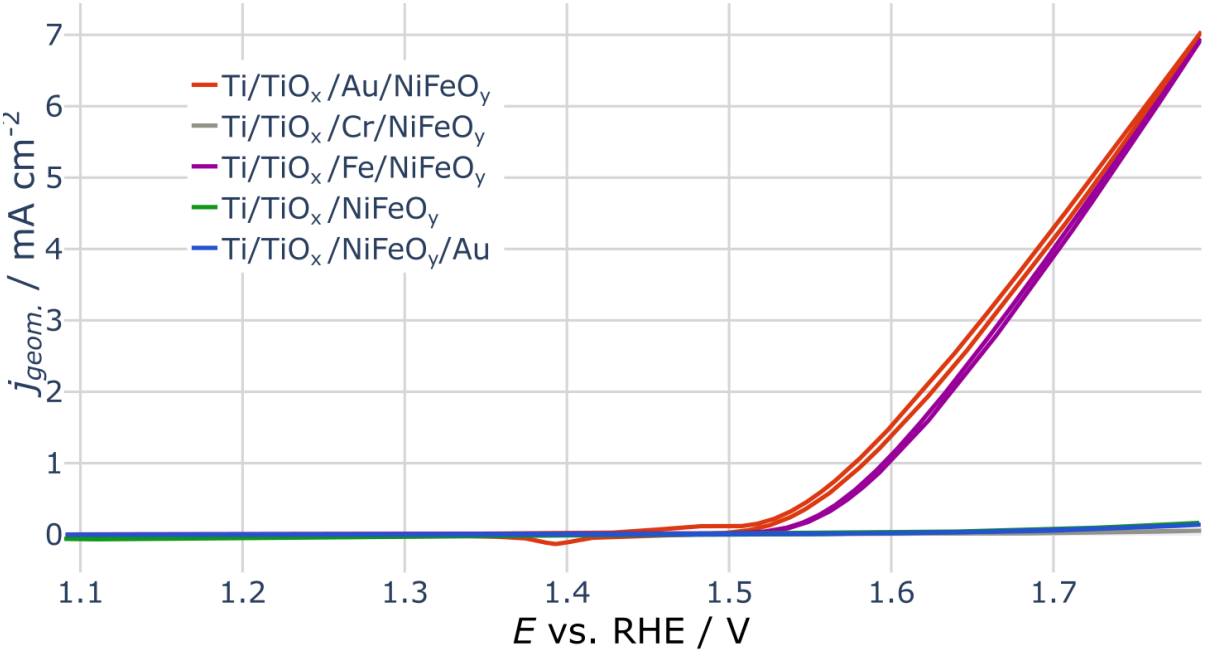

Fig. S 10: Comparison of all the interlayers used for the thin film investigations, within the same preparation batch. Each interlayer was prepared to be approximately 2 nm thick. Additionally one sample was prepared where a gold layer was deposited ontop the catalyst (blue line)

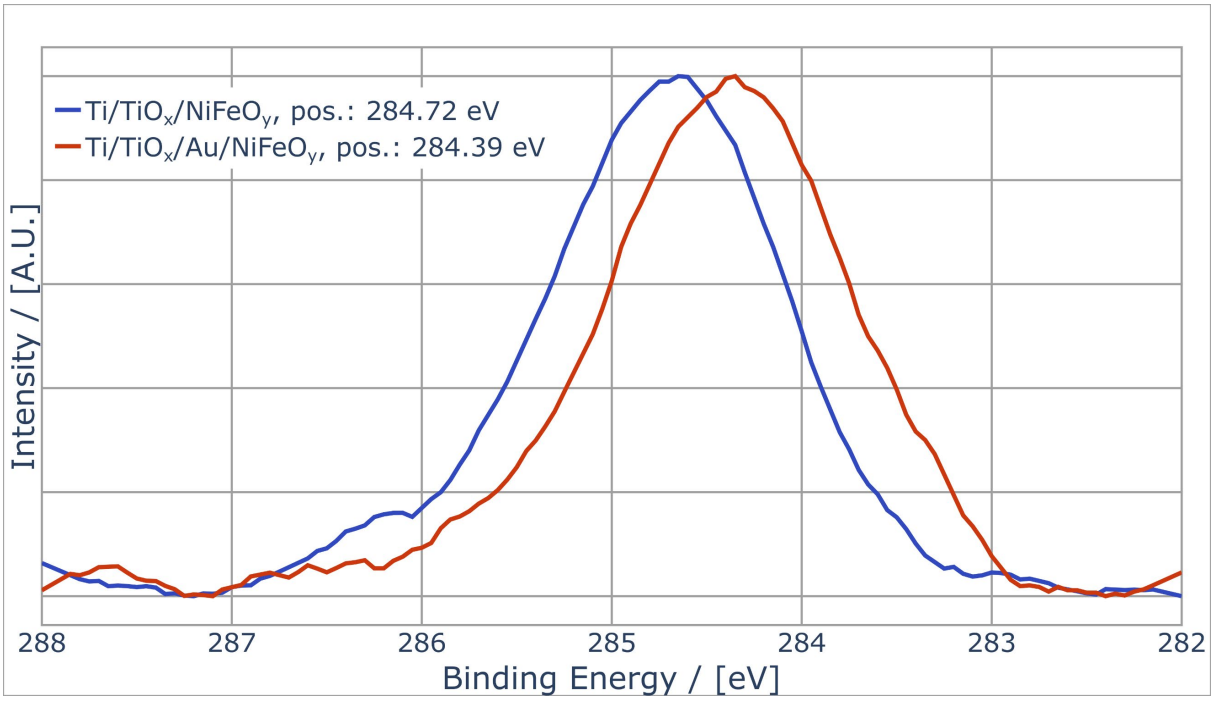

Fig. S 11: C 1s detail spectra of adventitious carbon after activation for the systems Ti/TiO_x /$NiFeO_y$ (blue) and $Ti/TiO_x/Au/NiFeO_y$ (red). For the as prepared catalyst films there was no adventitious carbon present as they were prepared under UHV.

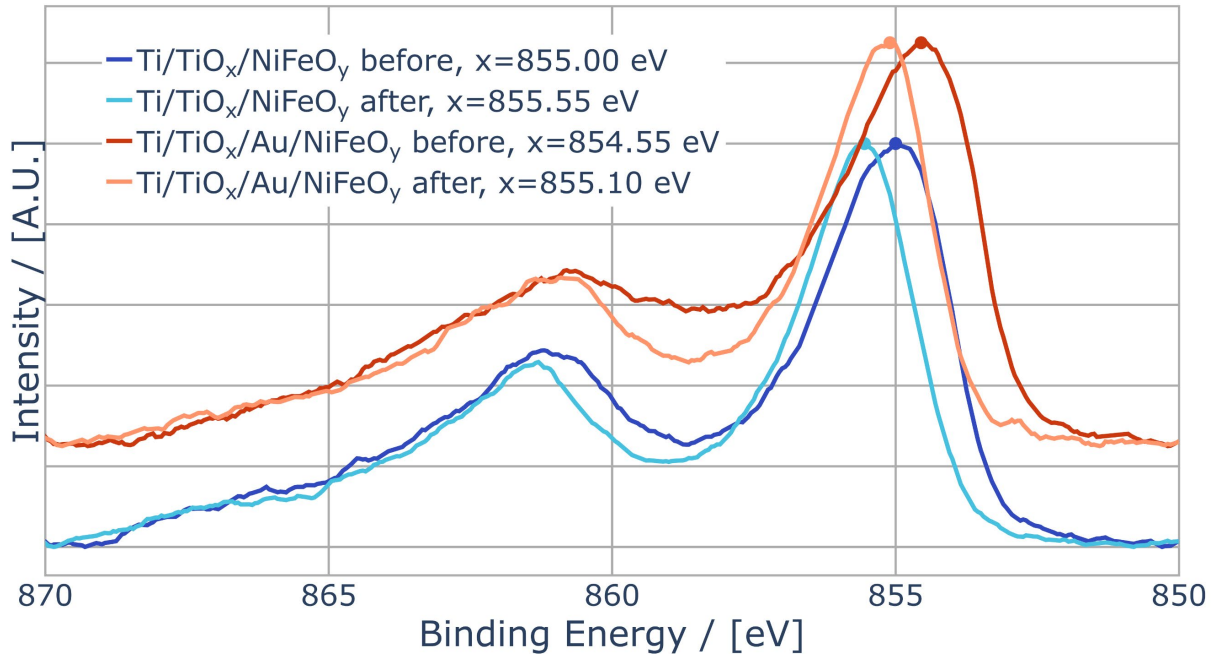

Fig. S 12: Ni $2p_{3/2}$ detail spectra from Figure 5 shown before calibration of the C 1s peak to 285 eV. For comparison the peak positions are given as dots and in the legend.

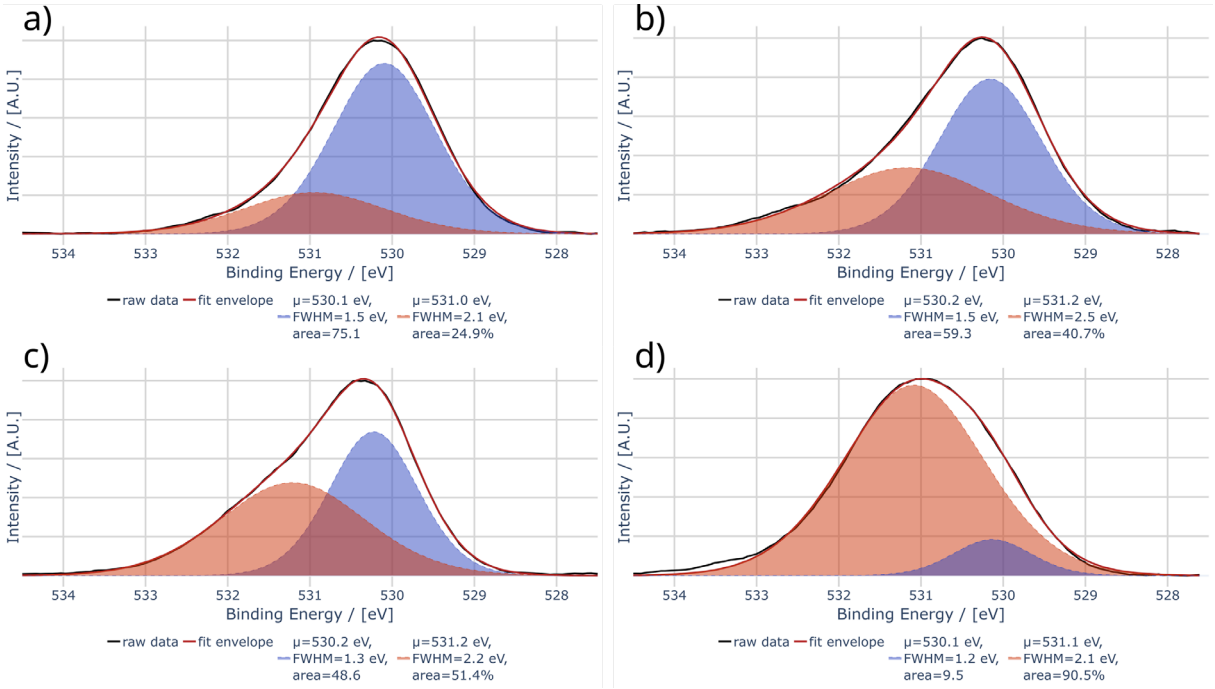

Fig. S 13: Plots from Fig. 7 shown together with the fit parameters. O 1s detail spectra for a) $Ti/TiO_x/NiFeO_y$ before and c) after activation; O 1s detail spectra b) $Ti/TiO_x/Au/NiFeO_y$ before and d) after activation. The black curve shows the smoothed raw data, the red curve indicates the envelope of the summed pseudo Voigt profiles.

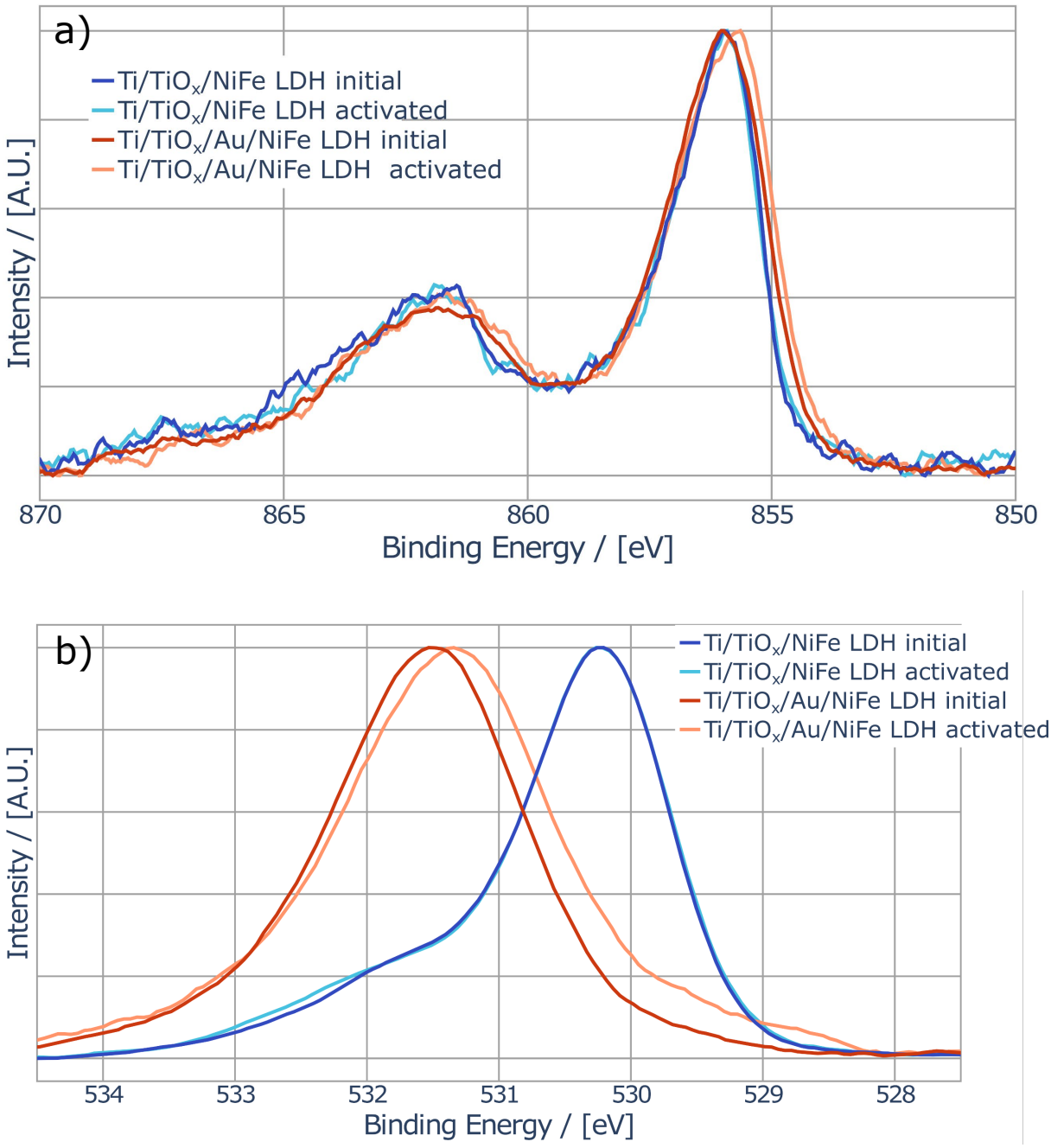

Fig. S 14: XPS of the Ni $2p_{3/2}$ a) and the O 1s b) spectra of solvothermally prepared NiFe LDH. The energies were calibrated to the C 1s peak at 285 eV. Initial refers to the samples after solvothermal preparation and activated refers to the samples after electrochemical treatment analogue to the thin film samples. This treatment does not seem to produce major changes in the samples as they already reached a phase that is stable in the used aqueous solutions for the investigated potential range.

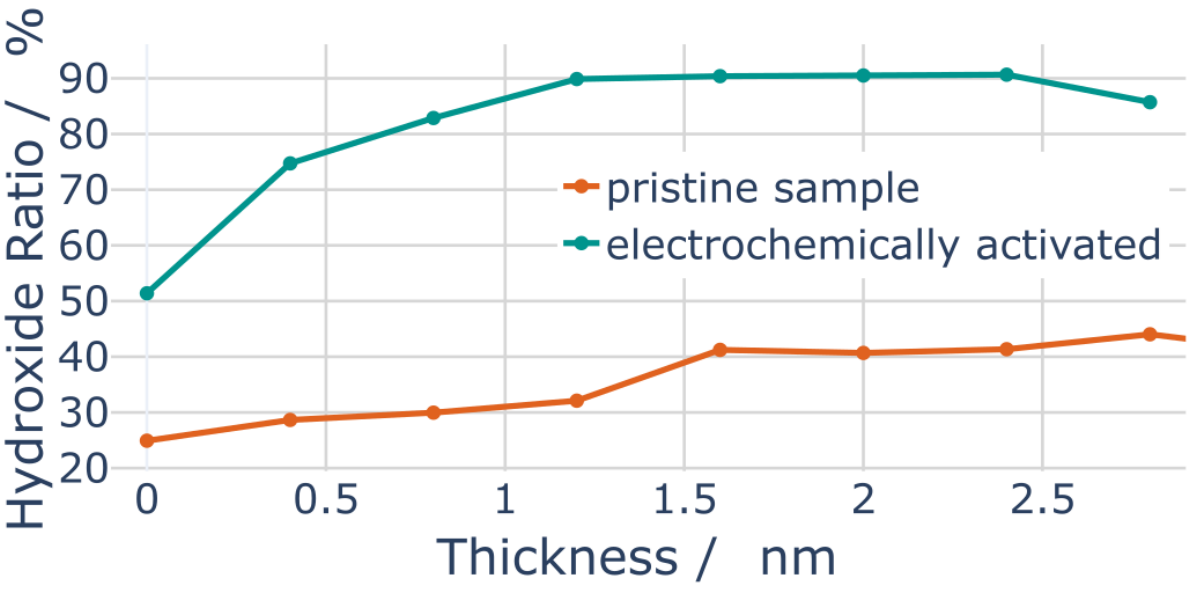

Fig. S 15: Ratio of low binding energy O1s component to high binding energy O1s component vs thickness of the gold layer for the thin film samples before and after electrochemical treatment, which leads to a strong increase in the high binding energy signal, that can be assigned to a higher oxidized $NiFeO_x(OH)_y$ species.

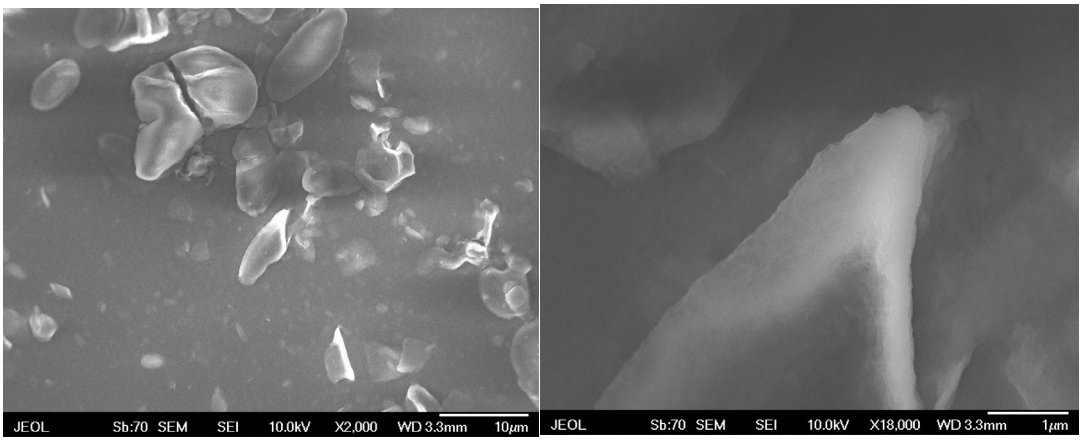

Fig. S 16: SEM pictures of NiFe LDH loaded onto a $Ti/TiO_{x,nat.}/Ni$ (10s) electrode. In contrast to the electrodes used for RDE measurements, no binder was added to the catalyst layer. We note that due to NiFe LDH's poor conductivity in the dry state, SEM pictures with high detail are difficult to produce.